https://dx.doi.org/10.1016/j.ymssp.2024.111268

Interface Behaviors of Elastic-plastic Waves and Its Impact on Uncertainties in Vibro-acoustic Modulation (VAM) for Structural Health Monitoring (SHM) of Bolt Loosening

Jianbin Li[1], Bo Wen[1], Zhen Zhang[1,*], Qian Li[1], Yi He[2], Zhongqing Su[2]

1 School of Aerospace Engineering and Applied Mechanics, Tongji University, Shanghai, China
2 Department of Mechanical Engineering, the Hong Kong Polytechnic University, Hong Kong, China
* Correspondence: 2013_tjzhangzhen@tongji.edu.cn

Highlights

- A novel theoretical model of interfacial stiffness for interface behavior of elastic-plastic waves.
- Physical explanations for causes and affecting factors of non-monotonic VAM behavior.
- Technical recommendation to retain the monotonic variation of VAM index during bolt loosening.

Abstract

The non-monotonic relationship between nonlinear VAM features and the residual torque of bolted joints has been experimentally observed in previous studies. Such non-monotonicity leads to the misjudgment in the quantitative SHM of bolt loosening. However, the causes leading to the non-monotonic behavior are unclear and an effective theoretical explanation is still lacking. To circumvent this deficiency, the interface behaviors of elastic-plastic waves are investigated in this study via theoretical modelling, simulation and experiment. A new exponential theoretical stiffness model is proposed to quantitively consider the effect of both surface roughness and interfacial pressure on the plastic asperity softening, in which roughness-related parameters are also incorporated in the exponent. The non-monotonic nonlinear VAM features are then predicted by both single-degree-of-freedom and multi-degree-of-freedom wave-surface interaction models. The effect of initial surface roughness and its variations caused by repeated loading on VAM features are validated by comparative experiment involving tightening tests of the aluminum-aluminum joint and the CFRP-CFRP joint, and retightening tests of the latter, respectively. The results show that the non-monotonicity of nonlinear VAM features is primarily influenced by the distribution of rough asperities on joint surfaces, and the different patterns of such non-monotonicity can be described by the proposed model. Higher model parameters indicate a rougher interface and result in more significant non-monotonic nonlinear VAM features. Retightening of rough joints can smoothen the contact surface. Following this guidance, the monotonic monitoring range of the CFRP-CFRP joint (Sa=5.362) has been improved from 11 N·m to 20 N·m after 16th bolt retight.

Keyword: bolt loosening, elastic-plastic behavior, contact acoustic nonlinearity, retightening, surface roughness

1 Introduction

Bolted joints are widely used to connect components in numerous engineering structures. Particularly, with the rapid advancement and the increasing application of composite structures, bolted connections have gained significant favor due to their convenience and ability to introduce fewer residual stresses [1]. However, bolts are frequently subjected to inevitable loosening due to time varying external loads during service, which will reduce structural reliability and even cause structural failure [2, 3]. Therefore, monitoring the residual preload of bolts is of great significance to ensure the mechanical performance of structures [4].

VAM is a method that has been increasingly investigated for the SHM of bolt loosening in the past decade. The VAM technique adopts two excitation signals on the bolted structure, namely low frequency (LF) pumping wave and high frequency (HF) probing wave. Subsequently, nonlinear structural responses, i.e., sidebands (SBs) at frequencies equal to the difference and sum of the frequencies of the two excitations, generate due to structural nonlinearities. When the interface of the bolted joint follows an elastic behavior, the contact acoustic nonlinearity (CAN) dominates the amplitude variation of SBs, which has a more significant correlation with the bolt loosening compared with linear acoustic features [5, 6]. The ratio of the amplitude of the SBs to the fundamental waves (LF and HF), known as the nonlinear modulation index β, has been widely used to evaluate the residual preload of the bolted joints. Amerini and Meo [7] first conducted VAM test on the evaluation of bolt loosening, the nonlinear modulation index β showed a monotonic correlation with the residual torque on the metallic joint. Zhang et al. [8] established a theoretical model based on the rough-surface contact theory [9] to link the VAM responses of a loose bolt to its residual torque and experimentally evaluated the bolt loosening of metallic and composite joints. Meyer and Adams [10] proposed an impact modulation method, which replaced the LF excitation of VAM by an impact, to identify the presence of loose bolts in a muti-bolted satellite structure. Wang and Song [11, 12] proposed several modifications (e.g., transducer, excitation and signal processing) on the traditional VAM method to increase the accuracy of the torque evaluation in multi-bolt connections. Gong et al. [6] established an extended theoretical model to describe the generation of high-order SBs based on CAN theory [9], and the high-order SBs were experimentally proved to have great potentials in detecting bolt loosening as well as the other small contact-type damages, such as micro fatigue crack, debonding and bond-slip.

Based on the classical CAN theory, the nonlinear modulation index β decreases monotonically with the increase of the preload for bolted joints tightened at an elastic stage. However, the non-monotonic behaviors of β (and the other similar indices based on the energy of nonlinear components) during the bolt loosening have been successively reported by recent studies. Zhao et al. [13] conducted repeated VAM experiments for the bolted joints under different torques (far less than the yielding strength of the jointed material), and the nonlinear modulation index β showed an increase at the initial stage of bolt preloading before its monotonic decrease for the higher torque. In addition, Nikravesh et al. [14] reported a bounce behavior of nonlinear modulation index after the bolt preload became relatively high. More comprehensive experiments were implemented by Qin et al. [1] to investigate the nonlinear modulation

intensity throughout the full-range loosening of the bolted structure. The nonlinear modulation index (an energy ratio of SBs to fundamental waves) also increased at a relatively low torque, and then decreased as expected by the existing theory, lastly followed by a similar bounce for the high-stress stage. Even though the above studies have been conducted through different conditions (e.g., material, size and excitation), a unanimous conclusion can be reached that the theoretical behavior for the nonlinear modulation index of monotonic decrease is confined to a middle-stress range. When the preload of the joint turns into an "edge case" (relatively high or low), the correlation between the nonlinear modulation index and bolt loosening may become more complex than that expected in the existing theory. Interestingly, such pattern can be found in not only the bolt loosening, but also the other damages, such as crack [15-17] and delamination [18, 19].
The non-monotonic behaviors of the nonlinear VAM features can lead to a misjudgment on the identification of the remaining torque at the bolted joint, because the single value of measured feature can refer to multiple stress levels.

To circumvent such uncertainties of the non-monotonic nonlinear modulation index in the structural health monitoring, some implements are used to obtain the monotonic indices for VAM testing. Li et al. [16] proposed to adjust the phase threshold range to improve the reliability of the relationship between the nonlinear modulation index and crack length. Zhao et al. [13] used the bi-spectrum energy as an alternative index of modulation to increase the accuracy of bolt loosening monitoring. Qin et al. [1] obtained a more monotonic early-loose warning by measuring the HF dissipation, compared to the nonlinear modulation index. However, the reported improvements, as replacements of the classical nonlinear modulation index, have only been restricted within the specific experimental conditions. The major factor contributed to the non-monotonic behavior in VAM responses is unclear and an effective theoretical explanation is still lacking, which limited the targeted improvements of the VAM method on the quantitative monitoring of bolt loosening. In addition, most of the bolted joints are supposed to be frequently retightened in their entire-life service, due to the inevitable loosening when confronting the cyclic loading [20]. Hence, the interfacial conditions of bolted joints are different from each other over the retightening process, leading to the more complicated fluctuations of the VAM features.

To improve the feasibility of the VAM method in the quantitative monitoring of bolt loosening, this article proposed a new model considering the elastic-plastic stiffness softening to explain the non-monotonic behavior of VAM responses and revealed the causes contributed to the detectable range of the nonlinear modulation index. Fig. 1 briefly shows the article structure. In Section 2, the elastic-plastic softening of interfacial stiffness was revealed by an indentation test. Based on such observed pattern, an exponent-decreasing stiffness model was proposed in the theoretical modeling to qualitatively explain the non-monotonic VAM behavior. Next, the present stiffness model was quantitively investigated and validated via experiments and finite element method (FEM) in Section 3. In Section 4, the nonmonotonicity of β affected by interfacial roughness was revealed through a comparison between aluminum-aluminum joint and composite-composite joint, and connected to the model parameters through the retightening tests, resulting in suggestions to improve the SHM accuracy of bolt loosening.

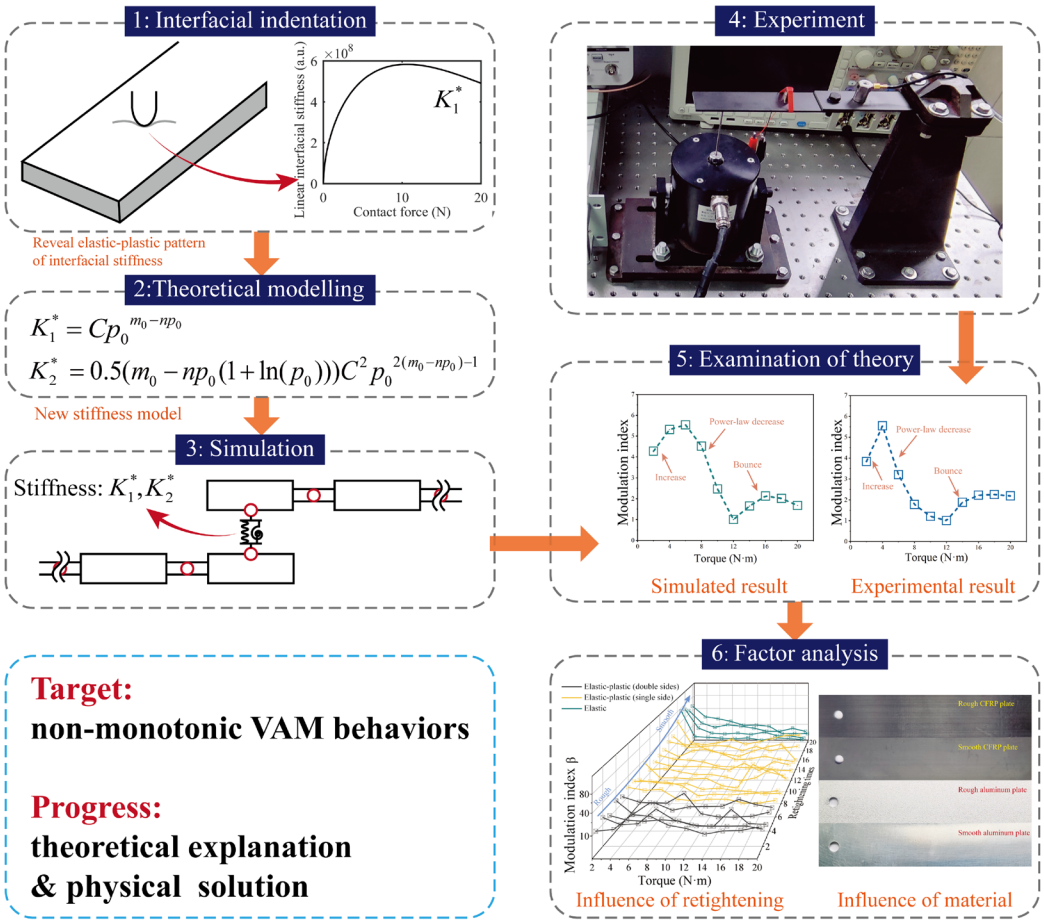

Fig. 1. Research flowchart.

2 Theory

2.1 Elastic-plastic behavior of rough contact surfaces

At the contact surface of a bolted joint, the applied compression is suffered by interfacial rough asperities, hence the regional deformation of the rough asperities dominates the interfacial stiffness of bolted joint. The interfacial stiffness of a bolted joint varies with changes of preloaded contact force, leading to the changes of the structural VAM responses. Hence, the measured VAM features can be used to monitor the loosening state of the bolted joint. The bolted structure can be simplified to a spring model in Fig. 2. The two plots of stiffness patterns are the representative forms of the linear interfacial stiffness in the elastic and elastic-plastic cases respectively. The elastic pattern is plotted based on Biwa's model [9] and the elastic-plastic pattern (stiffness softening) is plotted based on the proposed model in Section 2.2. As the result of the theoretical assumption, the interfacial stiffness shows a more significant plastic pattern for the rougher surface and shows an ideal elastic pattern for the smoother surface. Such conclusion will be validated in Section 4.

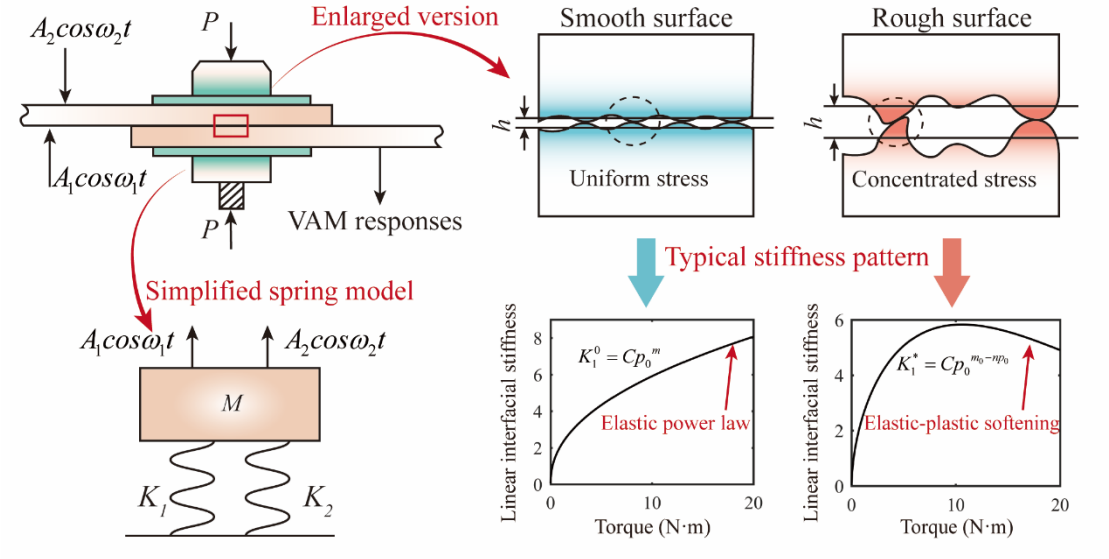

Fig. 2. Simplified model of a rough-contact joint subject to two harmonic forces.

The relationship between the preloaded contact force P and applied torque T in a bolted joint can be described by

$$P = T/(\tau d), \tag{1}$$

where τ is the coefficient of thread friction and d is the diameter of the bolt. Subjected to the preload of tightened bolt, the interfacial asperities suffer the contact pressure p, which obeys a functional relationship with the corresponding gap distance h, which has been defined as the opening distance between average planes of the upper and lower rough surfaces. The total distance h can be described as the sum of the initial distance h_0 caused by the static pressure p_0 (defined as the average pressure of the bolted region) and the relative displacement pumped by the waves (namely Δh), i.e.,

$$h = h_0 + \Delta h. \tag{2}$$

In the case of VAM test, the distance change caused by the excitations is relatively small compared to the static deformation of the compressed interface. Hence, the interfacial contact pressure $p(h)$ can be expressed by its Taylor expansion, i.e. [9],

$$p(h) = p(h_0 + \Delta h) = p_0 - K_1\Delta h + K_2\Delta h^2. \tag{3}$$

It can be seen from Eq. (3), when the bolted joint suffered the external excitation, the corresponding linear and nonlinear dynamic deformation will depend on the interfacial stiffness K_1 and K_2. Biwa et al. [9] has proposed a classical elastic model where K_1 follows a Hertzian power law (represented by K_1^0 in Fig. 2), and as a result, the nonlinear feature monotonically decreases with the increase of contact force. Despite numerous successful SHM applications of Biwa's model, the non-monotonic nonlinear features due to bolt loosening at different degrees [9-11] cannot be accurately described by such elastic model. Recently, numerous advanced models [21] have been proposed to describe the elastic-plastic CAN behaviors, e.g., fractal model [22] and GW model [18], using statistic functions to describe the asperity characters. However, there is still no universal theory for the reported elastic-plastic VAM behaviors [1, 13, 14] caused by bolt loosening, and most of the models [18, 22] based on complicated functions have also raised their application threshold. Hence, we seek to conceive a new model with a simple form as well as an effective function to describe the elastic-plastic VAM behavior

in the bolt loosening monitoring. The new elastic-plastic linear and nonlinear interfacial stiffness are denoted as K_1^* and K_2^* respectively. For Eq. (3), they satisfy that

$$K_1^*=K_1=-\frac{\mathrm{d}p}{\mathrm{d}h}\Big|_{h=h_0}, \tag{4}$$

$$K_2^*=K_2=\frac{1}{2}\frac{\mathrm{d}^2p}{\mathrm{d}h^2}\Big|_{h=h_0}. \tag{5}$$

An indentation test on the material surface was conducted to reveal the elastic-plastic pattern of the interfacial stiffness (K_1^* and K_2^*) affected by the stress concentration. A plate used for VAM evaluation on bolt loosening in the following sections was tested. The tested plate was made by press molding using CFRP, of which the material and geographic parameters were listed in Table 1. The setup of indentation test is shown in Fig. 3a. A compression machine (WANCE®) with a force sensor was used to control the contact force between the material surface and the spherical indenter. The displacement control mode was used to apply the indentation load. The maximum indentation depth was set as 0.02 mm, larger than the maximum deformation in the bolted composite joint tightened by 20 N·m, but smaller than the material yielding deformation (0.026mm). The interval of loading depth was 0.028 μm and the loading speed was 1 mm/min.

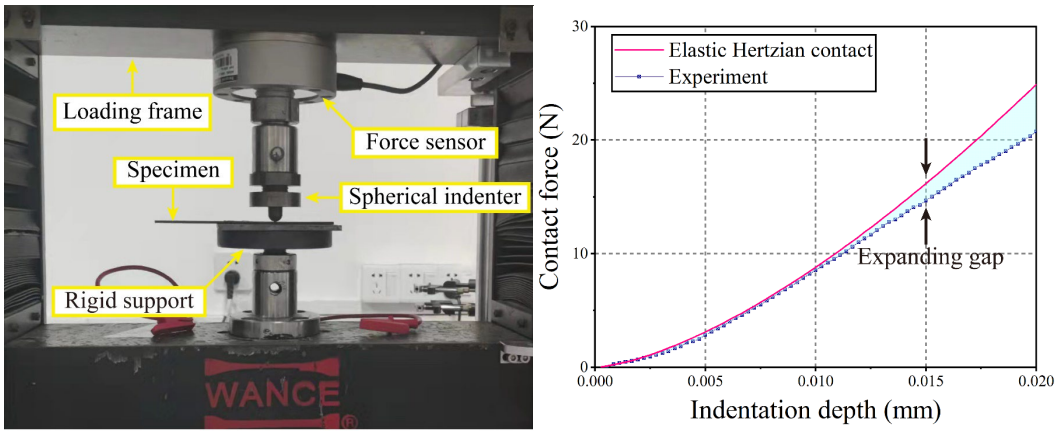

a) Setup for the indentation test b) Measured contact force over indentation depth

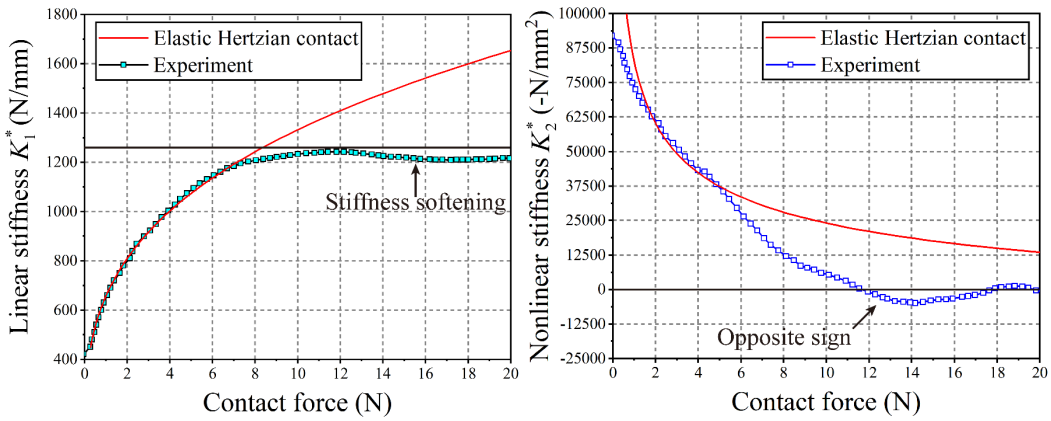

c) Measured K_1^* over contact force d) Measured K_2^* over contact force

Fig. 3. Interfacial stiffness measurement of rough composite samples.

The result of contact force was plotted in Fig. 3b. A theoretical curve based on elastic Hertzian

law ($h \propto P^m$) was fitted using the experimental data over a depth from 0 to 0.01 mm for reference. The measured contact force shows an expanding drop compared with that in elastic contact, which indicates a stiffness softening due to elastic-plastic contact. Next, according to Eqs. (4) and (5), the interfacial stiffness K_1^* and K_2^* in the loading test was obtained as the derivatives of the curve of contact force versus indentation depth. The elastic-plastic stiffness K_1^* and K_2^* measured in the experiment (Fig. 3c and Fig. 3d) were also fitted based on the elastic Hertzian law to obtain a reference. In Fig.3c, K_1^* does not follow the elastic Hertzian law after the contact force become larger than 8 N. K_1^* rises to a peak at 12 N and followed by a softening behavior. When K_1^* reaches its highest value (contact force=12 N), K_2^*, as a derivative of K_1^*, is equal to 0 in Fig. 3d. Then K_2^* shows an opposite sign to restrain the softening of K_1^* and lastly K_2^* converges to 0.

Table 1. Material and geographic parameters of the CFRP plate.

Layup	**Elasticity modulus *E*(GPa)**	**Poisson's ratio *v***	**Density (kg/m^3) *ρ***	**Frictional coefficient *τ***
$[90,0,90,0]_{2s}$	$E_1/E_2/E_3$	$v_{11}/v_{13}/v_{23}$	1700	0.2
	130/7/7	0.32/0.32/0.45		

2.2 A new elastic-plastic model of wave interaction with rough contact interfaces

Since the contact surface of the plate shows a significant elastic-plastic behavior with the variation of contact force, the corresponding VAM responses will be different from the past interfacial stiffness models. Hence, a new model of the interfacial stiffness is proposed in this paper, in which the form of K_1^* in Eq. (4) is designed as

$$K_1^* = Cp_0^{\,m_0 - np_0}, \tag{6}$$

where C is a scale factor which has little influence on the monotonicity of the VAM behavior, m_0 represents the initial power exponent for interface without compression and n represents the nonnegative softening factor respectively. Given Eq. (6), the nonlinear interfacial stiffness K_2^*, as the derivative of K_1^*, can be obtained as

$$K_2^* = 0.5(m_0 - np_0(1+\ln(p_0)))C^2 p_0^{\,2(m_0-np_0)-1}. \tag{7}$$

The influence of the wide-range variation of preload on the elastic-plastic deformation of the contact asperities is simulated by introducing the term of "$-np_0$". When softening factor n=0, Eq. (6) is degenerated into Biwa's model [9] (i.e., $K_1^0 = Cp_0^{\,m}$). Following the reported conclusions [9, 23], the physical meaning of m_0 can be described as the initial roughness condition of the interface when the bolt preload is not applied. The height of the contact asperity will decrease faster under compression for a larger value of n. The combined contribution of the proposed parameters dominates the pattern of interfacial stiffness from low-stress contact to high-stress contact (i.e., the full range of bolt loosening).

Then, based on the present model, we have the modification of the equation [9] of nonlinear motion of the joint subject to the two excitation forces:

$$M\ddot{x} + K_1^* x - \varphi K_2^* x^2 = A_1 \cos\omega_1 t + A_2 \cos\omega_2 t, \tag{8}$$

where ω_1 and ω_2 are the frequencies of the pumping vibration and probing wave respectively.

φ is a small quantity to scale the perturbation to be minute. Considering the form of first-order nonlinearity for Eq. (8), the displacement solution can be solved using the perturbation method [8, 9]. As a result, the solution x for Eq. (8) includes the linear fundamental waves (x_{HF} and x_{LF}) and the modulated sidebands (x_{LS} and x_{RS}), as

$$x_{LS} = \frac{A_1 A_2}{K_1^* - M(\omega_1 - \omega_2)^2} K_2^* \cos(\omega_1 - \omega_2)t = A_{LS} \cos(\omega_1 - \omega_2)t\,, \tag{9}$$

$$x_{RS} = \frac{A_1 A_2}{K_1^* - M(\omega_1 + \omega_2)^2} K_2^* \cos(\omega_1 + \omega_2)t = A_{RS} \cos(\omega_1 + \omega_2)t\,, \tag{10}$$

$$x_{HF} = \frac{A_1}{K_1^* - M\omega_1^2} \cos\omega_1 t = A_{HF} \cos\omega_1 t\,, \tag{11}$$

$$x_{LF} = \frac{A_2}{K_1^* - M\omega_2^2} \cos\omega_2 t = A_{LF} \cos\omega_2 t\,, \tag{12}$$

To reduce the influence of excitation amplitudes (i.e., A_1 and A_2) on damage evaluation, the nonlinear modulation index β is always described by the ratio of nonlinear amplitudes to linear amplitudes, i.e.,

$$\beta = \frac{(A_{LS} + A_{RS})}{2A_{HF}A_{LF}} = \frac{0.5K_2^*}{K_1^* - M(\omega_1 - \omega_2)^2} + \frac{0.5K_2^*}{K_1^* - M(\omega_1 + \omega_2)^2}. \tag{13}$$

Based on Eqs. (6), (7) and (13), the VAM response mainly depends on the interfacial stiffness, i.e., the interfacial contact pressure or the applied torque in the bolted joint.

To discuss the roles of different parameters in the present model, the theoretical results of interfacial stiffness (Eqs. (6) and (7)) and corresponding nonlinear modulation index (Eq. (13)) are calculated in the case of single-degree-of-freedom (SDOF) contact of bolted joint. The input parameters (e.g., mass and frequencies) are the same as those used in the experiment in Section 3.1. The calculated theoretical results are shown in Figs. 4 and 5.

2.2.1 Influence of m_0 on interfacial stiffness and nonlinear modulation index β

m_0 mainly dominates the behaviors of the interface at the beginning of loading. When the power exponent of K_2^* in Eq. (7) $2(m_0 - np_0) - 1 > 0$ (for example, m_0=0.55 in Fig. 4), K_2^* and β show an increasing trend from 0 to 5 N·m and then decline with the increase of the torque due to the softening effect. Such non-monotonic increase of K_2^* and β at the initial stage of contact loading has also been reported by some theoretical researches [22, 24], and could be explained as the increase of the interfacial contact area [25]. In contrast, when m_0 is small enough (for example m_0=0.35 in Fig. 4), which physically means the surfaces with more uniform asperity heights, the corresponding K_2^* and β follow an elastic behavior of monotonic decrease even at the low-stress stage, as is expected in Biwa's model. In addition, a larger m_0 can lead to a higher bounce at the high-stress stage.

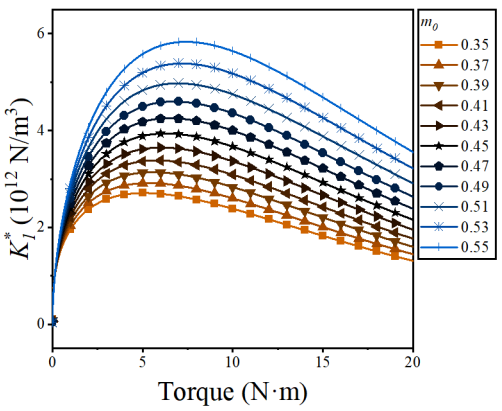

a) Linear interfacial stiffness K_1^*

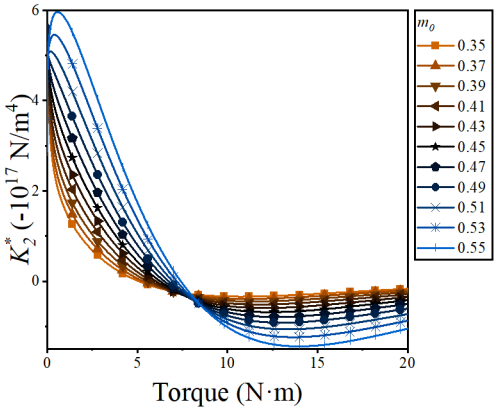

b) Nonlinear interfacial stiffness K_2^*

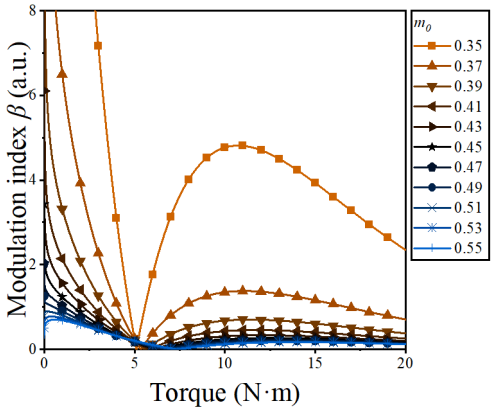

c) Modulation index β

Fig. 4. Theoretical interfacial stiffness and modulation index of SDOF bolted composite joints over a torque range from 0 to 20 N·m and a range of m_0 from 0.35 to 0.55, with n set to 0.002.

2.2.2 Influence of n on interfacial stiffness and nonlinear modulation index β

The influence of the softening parameter n rises with the increase of the preload. When n=0, K_1^*, K_2^* and β follows the elastic power law as predicted by Biwa's model. When n≠0, for example, n=0.002 for Figs. 5a~c, the contact-dependent stiffness softening becomes significant. K_1^* increases from the low-stress level before reaching a peak at 5 N·m, and then slowly decreases for the increasing torque, as the same as the measured behavior in the indentation test (Fig. 3c). Similarly, K_2^* goes to 0 when K_1^* reaches its peak, and finally convergent to 0 (Fig. 3 d). As a typical VAM result caused by the stiffness softening, β in Figs. 5c show a bounce when n is nonzero. The larger parameter n leads to an earlier bounce. If n is relatively small, take n=0.0004 (in brown) for example, β rises at about 14 N·m and keeps rising in the rest of the load range (15 ~20 N·m). In contrast, although β for n=0.002 (in blue) will also show a bounce at 5 N·m, β will gradually drop after it reaches the highest peak near 10 N·m. This difference can be used to explain why the nonlinear modulation index in high-stress tightened joint for [14] show a gradual increase but that for [1] show a fall after its highest peak.

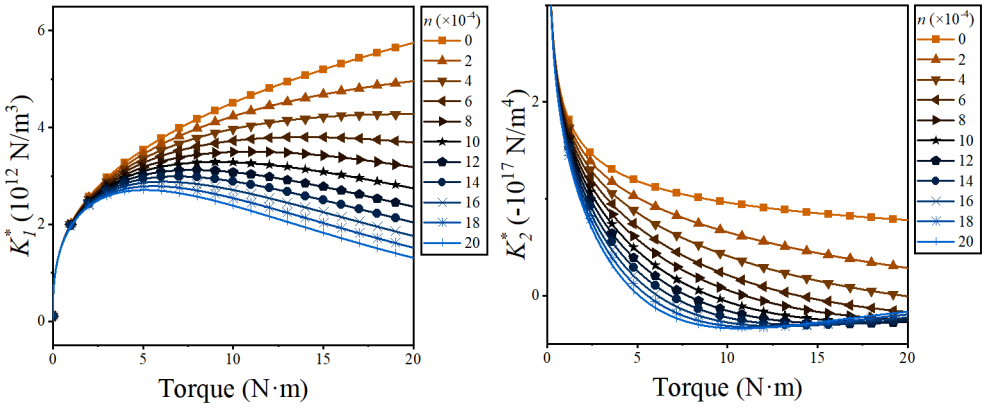

a) Linear interfacial stiffness K_1^* b) Nonlinear interfacial stiffness K_2^*

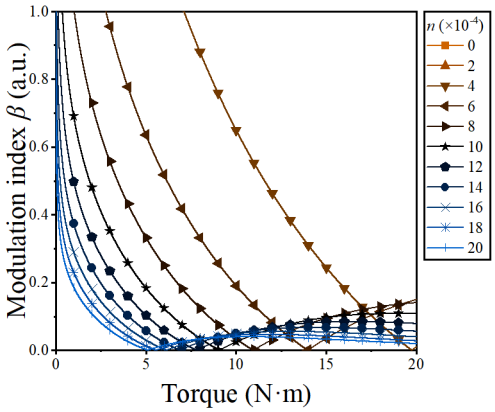

c) Modulation index β

Fig. 5. Theoretical interfacial stiffness and modulation index of SDOF bolted composite joints over a torque range from 0 to 20 N·m and a range of n from 0 to 0.002, with m_0 set to 0.35.

Over all, the softening effect on the contact asperities is of duality. A remarkable n represents the higher-speed collapse of contact asperity, which can drive β into the ideal decrease from the initial increase due to the increase of contact pairs [25]. However, a large n represents an over-speed plastic deformation of the asperities for high-stress level, leading to the earlier emergence of following bounce of β. In a word, higher n leads to an earlier high-stress bounce and diminishes the low-stress increase, while higher m_0 delays the high-stress bounce and enhance the initial increase of β.

The theoretical results indicate that the elastic behavior of monotonic decreasing β is now limited within a range from $p_{\min}$ to $p_{\max}$, by satisfying the following necessary conditions. For the low-stress stage (e.g., m_0=0.55 for Fig. 4), the increase of β is due to the increase of K_2^*, that is to say, the exponent of Eq. (7) >0 (i.e., $2(m_0 - np_0) - 1 > 0$). Meanwhile, the reason of high-stress bounce (e.g., n=0 and n=0.002 for Fig. 5) can be ascribe to the stiffness softening of K_1^*. When K_1^* begins to decline, K_2^*, as the derivative of K_1^*, equal to 0. That is to say, the primary term $m_0 - np_0(1+\ln(p_0)) > 0$. Therefore, the boundary condition for monotonic detection can be obtained as,

$$\begin{cases} 2(m_0 - np_{\min}) - 1 < 0 \\ m_0 - np_{\max}(1 + \ln(p_{\max})) > 0 \end{cases}. \tag{14}$$

Then we have the length of the monotonic detection range for the decreasing β as

$$p_{\max} - p_{\min} < \frac{\eta - 2m_0(\eta - 1)}{2n\eta}, \tag{15}$$

where η represents $(1 + \ln(p_{\max}))$ and η>1. According to Eq. (15), the detectable range for a reliable SHM is wider for a specimen with low m_0 (roughness) and low n (asperity plasticity). In addition, via solving Eq. (14), the conditions for the monotonic SHM can be obtained as

$$\begin{cases} 0 < m_0 \le \frac{1}{2} \\ 0 < n < \frac{m_0}{p_{\max} + p_{\max}\ln(p_{\max})} \end{cases}, \tag{16}$$

or

$$\begin{cases} \frac{1}{2} < m_0 \le \frac{p_{\max} + p_{\max}\ln(p_{\max})}{2(p_{\max} - p_{\min} + p_{\max}\ln(p_{\max}))} \\ \frac{2m_0 - 1}{2p_{\min}} < n < \frac{m_0}{p_{\max} + p_{\max}\ln(p_{\max})} \end{cases}. \tag{17}$$

Based on Eqs. (16) and (17), the monotonic range of VAM detection can be predicted theoretically after the model parameters of the used specimen have been measured, which provides a reference for the usage of VAM features in the SHM of bolt loosening.

The main innovative work of the proposed theoretical frame can be summarized as two points:

1) Past classical models [9, 22] focus on the accurate description of the initial interfacial condition, in which the exponents of the expression are constant. The present model has first used a continuity function of the variable p0 as the power exponent of Eq. (6), which enables the pressure-caused elastic-plastic behavior of the interfacial stiffness and the non-monotonical VAM response can be uniformly described.
2) Based on the expressions of the proposed model (Eqs. (6) and (7)), the theoretical monotonic range of VAM detection for the determined roughness condition (represented by model parameters) and the required roughness condition for a certain detection range have been obtained, which provides a promising reference for the SHM based on the VAM technique.

3 Experiment and simulation

The non-monotonic VAM behavior in the bolted joint during loosening has been investigated in the experiment and used to validate the present model with FEM.

3.1 Experimental setup and finite element model

Two same CFRP plates were connected using an M6 bolt, the estimated parameters for the plates were detailed in Table 1. The grade of the used bolt was selected as 12.9, with an ultimate tensile strength of 1200 MPa and a yield ratio of 0.9, on the purpose of avoiding the potential acoustic nonlinearity contributed by the plastic deformation of the bolt. The setup of experiment

is shown in Fig. 6 a. Firstly, the specimen was clamped by a holder and the preload of the bolt was applied by a torque wrench. Next, the LF pumping wave and HF probing wave were excited by a two-channel signal generator (Tektronix®, AFG 31000). The LF pumping wave was introduced on the specimen by a shaker (Donghua®, SH40020), amplified by an amplifier (Donghua®, DH5871). Simultaneously, the HF probing wave was introduced on the specimen by an actuator (PI®, P-885.11). Lastly, the response signals of the bolted joints under the mixed excitations were captured using an accelerometer (Donghua®, 1A115E) and outputted by an oscilloscope (Tektronix®, MDO 4034C). A sweeping frequency test was conducted to determine the excitation frequencies which can generate remarkable sidebands without causing structural resonance. As a result, the frequency of LF excitation was 215 Hz and the frequency of HF excitation was 29.8 kHz. The sampling frequency of the oscilloscope was 250 kHz. The non-monotonic VAM behaviors for experiment in this section was observed from the plates with smooth surfaces after being retightened for the 15th time. The influence of the interfacial roughness and the retightening progress will be discussed in Section 4.

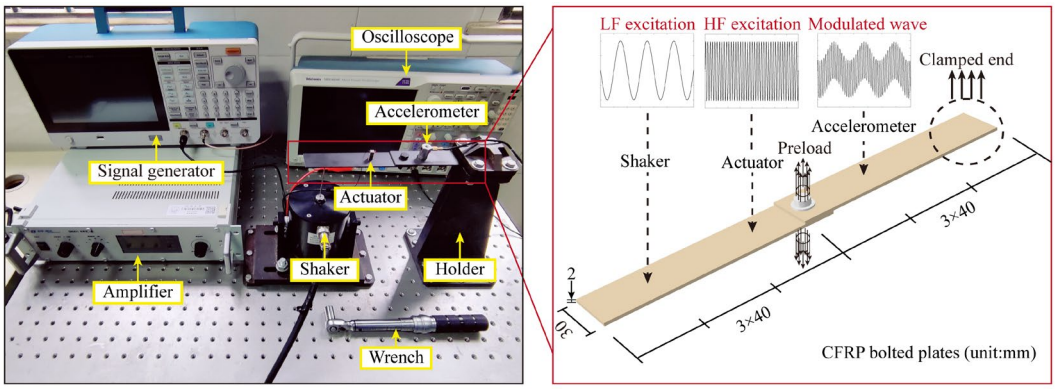

a) Experimental setup

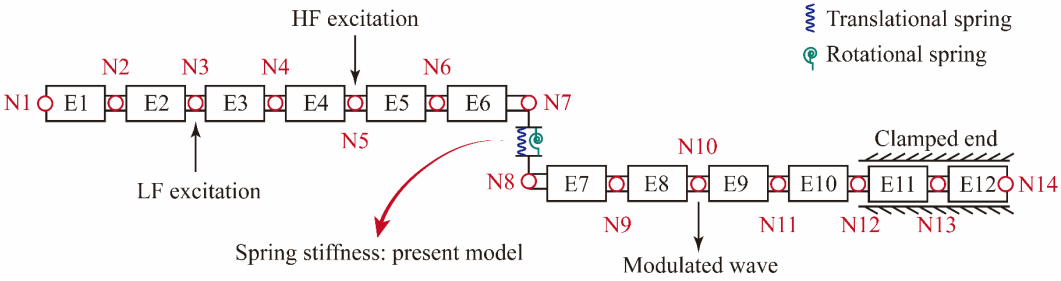

b) FE model

Fig. 6. Experimental setup and FE model for the bolted joint.

In the aim of validating the theoretical model, the result measured by experiment was compared with that by simulation using the present elastic-plastic stiffness model. The analytical results in Subsection 2.2 are based on a SDOF contact, hence a simulation is needed to consider the multi-degree-of-freedom (MDOF) interaction, boundary and propagation of VAM waves in a bolted joint during its loosening. A finite element (FE) model based on MATLAB was chosen to simulate the bolted structure. The refinement of the MDOF model over the SDOF model included: a) For the whole structure (Fig. 6 b), each node of the FE model had 2 degrees of

freedom (i.e., translation and rotation), that was to say, the simulated signals were caused by a MDOF structure. b) For the contact region, we used a single spring to connect the two beams, of which the translational stiffness was defined as the SDOF model in Section 2 and the rotational stiffness was defined in proportion to the translational stiffness. For the boundary, the clamped elements were simulated by making the nodes connected to them rigid, of which the translation and rotation were not allowed.

The parameters of the FE model including material, sizes, boundaries, loads and excitations were defined to match the experimental conditions. The model (Fig. 6 b) of the bolted joint was comprised by two Euler-Bernoulli beams. Each beam was meshed by 6 elements (E1~E6) with the same size and 7 nodes (N1~N7) with two degrees of freedom (transverse deflection and rotation). The area from N12 to N14 was clamped to make the whole structure a cantilever. To simulate the bolted connection, E6 and E7 were given the additional mass and connected by a translational spring and a rotational spring between N7 and N8. The stiffness of the translational spring (K_t) was defined according to the present model (Eqs. (6) and (7)), as

$$K_t = \begin{Bmatrix} K_1^* \\ K_2^* \end{Bmatrix} = \begin{cases} C{p_0}^{m_0 - np_0} \\ 0.5C^2(m_0 - np_0(1+\ln(p_0)))\,{p_0}^{2(m_0-np_0)-1} \end{cases}, \tag{18}$$

and the stiffness of the rotational spring K_r was defined in proportion to K_t [26], i.e.,

$$K_r = \alpha K_t = \begin{Bmatrix} \alpha K_1^* \\ \alpha K_2^* \end{Bmatrix}, \tag{19}$$

where α is a constant determined by experimental result. The stiffness of the two springs was then related to the interfacial pressure p_0, which realized the VAM simulation under different bolt preload.

A mixing excitation was introduced on the structure, consisting of the LF pumping wave (215 Hz) at N3 and HF probing wave (29.8 kHz) at N5. The VAM responses of the bolted joint under different residual torques, were iteratively solved based on Newmark's algorithm [26]. The structural dynamic responses were collected from N10. To achieve a balance between calculation time and accuracy, the running time for the simulation was 5 seconds and the sampling frequency was 100 kHz. The FE model did not take into account the combined contribution of the intrinsic nonlinearities [19], such as the local resonances, mode conversions, nonlinear dissipations, etc. Hence, this allowed for a clearer indication of the VAM responses in a bolted joint that was only dominated by the elastic-plastic contact.

3.2 Results

The signal features for the FEM and the experiment show a good agreement. In Fig. 7, the frequency spectra show that the excited HF wave is modulated by the LF wave, causing the generation of nonlinear sidebands, i.e., left sideband (LS) at 29.585 kHz and right sideband (RS) at 30.015kHz. The amplitudes for FEM and experiment consistently show the non-monotonic variation with the increase of the applied torque. By establishing a baseline at the peak of LS at 12 N·m, it is evident that the LS amplitude for 6 N·m and 16 N·m is higher than that of 12

N·m.

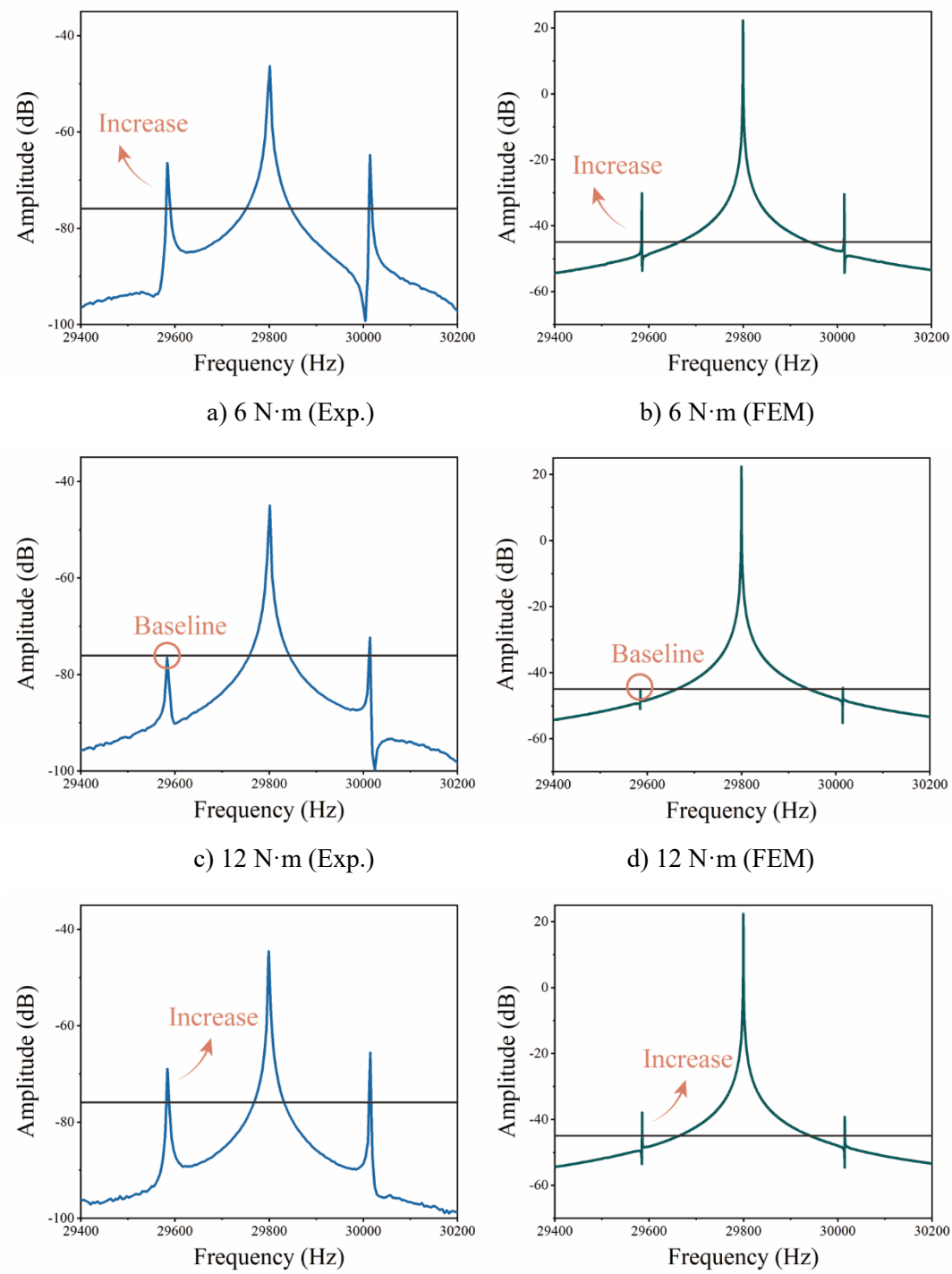

a) 6 N·m (Exp.) b) 6 N·m (FEM)

c) 12 N·m (Exp.) d) 12 N·m (FEM)

e) 16 N·m (Exp.) f) 16 N·m (FEM)

Fig. 7. Spectra of the modulated waves for experiment and FEM. a) ~c) experimental signals, d) ~f) simulated signals (C=4.9×10^6, α=1×10^3, m_0=0.78 and n=0.0035).

The detailed non-monotonic trends of SB peaks over the whole stage of bolt loosening are shown in Figs. 8a and b. The variation (in Fig. 8a) of the LS and RS amplitudes in the experiment differs from each other in contrast to that in FEM (Fig. 8b). Such difference results from the complex contribution of phase-dependent nonlinearity has not been involved in the

FE model, as mentioned in Subsection 3.1. Hence, a universal improvement for the SHM based on VAM is to use the mean value of LS and RS amplitudes to establish the nonlinear modulation index [8, 27]. Considering that the measured unit of signals in the FEM (m/s^2) is different from that in the experiment (V), the obtained β for Fig. 8 c and d are divided by their minimum respectively. The ratio of the sideband amplitude to the HF and LF amplitude for experiment is always higher than that for simulation, because there are some intrinsic nonlinearities caused in the experimental environment, such as the transducers and material, which can also generate sidebands but have not been considered in the FE model. However, the intrinsic nonlinearities will hardly change with the change of the preload, leading to little effect to the variation of VAM features over the investigated torque range.

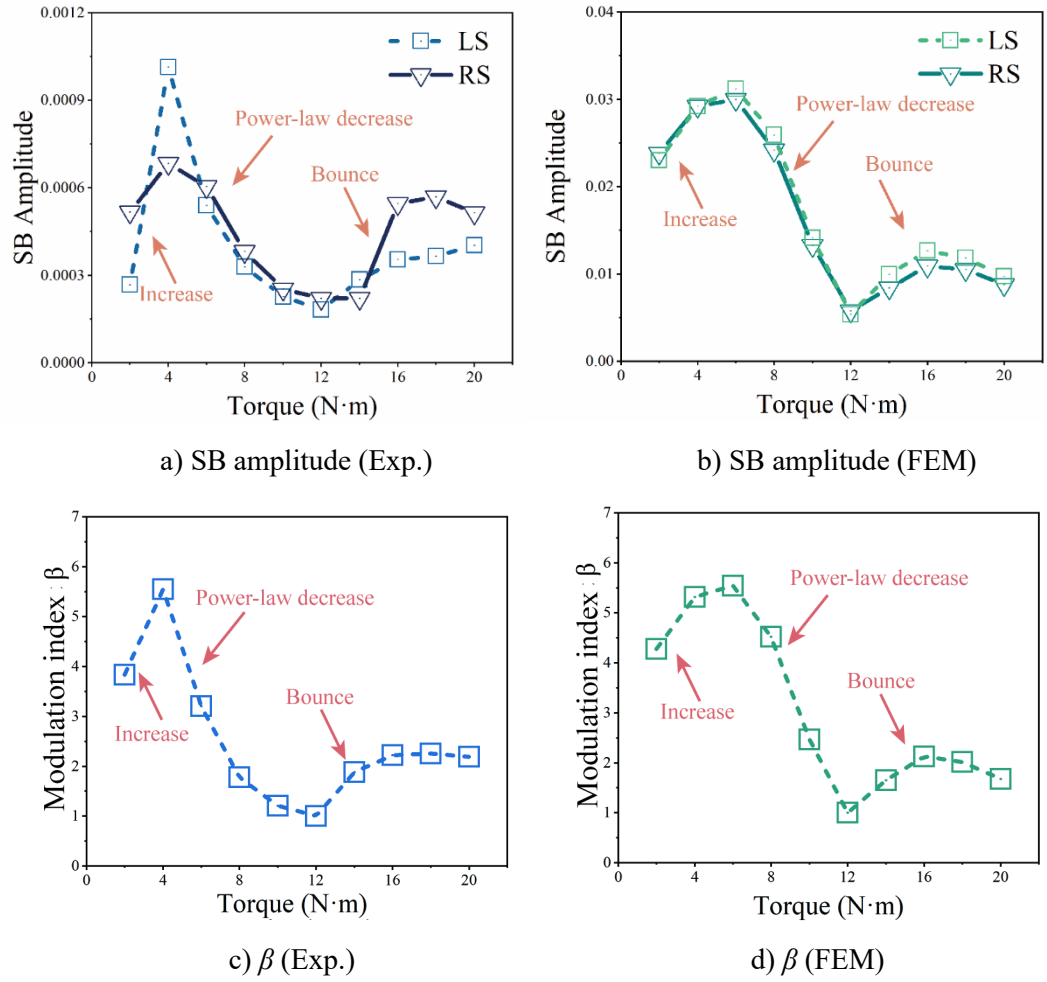

a) SB amplitude (Exp.)

b) SB amplitude (FEM)

c) β (Exp.)

d) β (FEM)

Fig. 8. Experimental and FEM results of VAM responses for the bolt loosening.

The nonlinear modulation index in the experiment shows a similar behavior with that in FEM based on the exponent-decreasing model (Figs. 8c and 8d), which validates the present model. At the beginning of preload, the nonlinear modulation indices for experiment and FEM increase temporarily. Then, they drop to the lowest by following the power law, as expected by the elastic Hertzian models [9]. The highest peak for Fig.8c is at 4 N·m but the highest peak for Fig.8d is at 6 N·m. This is because the rough asperities in the experimental setup are not completely in contact during the initial tightening, which differs from the assumption in the FEM. As the

preload increases, this difference can be reduced. After being tightened by a relatively high-stress torque (about 12 N·m), the nonlinear modulation indices begin to show a bounce to double folds of the lowest value and followed by a slow decline, as similar as the proposed model. Such double-sides non-monotonic behavior of the nonlinear modulation index has also been reported by [1], in which the applied torque on an M20 bolt varied from 5 to 140 N·m. Comparatively, the single-side non-monotonic nonlinear modulation indices reported by [13, 14] were generally based on a smaller range of the preload variation. Therefore, a reasonable conclusion can be obtained that the monotonic nonlinear modulation index only exists within a limited range of applied preload, as predicted by Eq. (15). The consistent results between the experiment and FEM also indicate that the interfacial stiffness softening subsequently leads to the non-monotonic VAM behavior (SB amplitude and modulation index).

4 Factor analysis

To avoid the misjudgment on the residual torque during SHM of the bolted structures, a monotonic nonlinear modulation index (or SB amplitude) relative to the torque is always required. Since the stiffness softening causes the VAM nonmonotonicity, the remaining task in this study is to find the factors resulted in the stiffness softening, and provide a physical solution for the quantitative SHM using VAM method.

4.1 Influence of material

To reveal the major factor affecting the VAM monotonicity, VAM evaluation of the residual torque for CFRP-CFRP (referred to as C-C) joints and aluminum-aluminum (referred to as Al-Al) joints were conducted respectively. Meanwhile, the surfaces for each material consisted of two kinds of roughness, i.e., rough surface and smooth surface. For the C-C joint, the difference of roughness was realized via changing the roughness of the mold during the formation of specimens. For the Al-Al joint, the rough surface was made by the shot blasting. Except the roughness, the plates for each material have the same material and size. The VAM signals on the four specimens during the bolt tightening were detected based on the same experimental measurement (e.g., frequency, boundary condition, equipment, etc.) introduced in Section 3.1 and Figure 6a. Fig. 9 shows the measured modulation index of the four specimens. Additionally, the surface morphology with the area of 1 mm^2 of each specimen before loading was measured with a 3D profile tester (Filmetrics®, Profilm 3D) and inserted in Fig. 9, respectively.

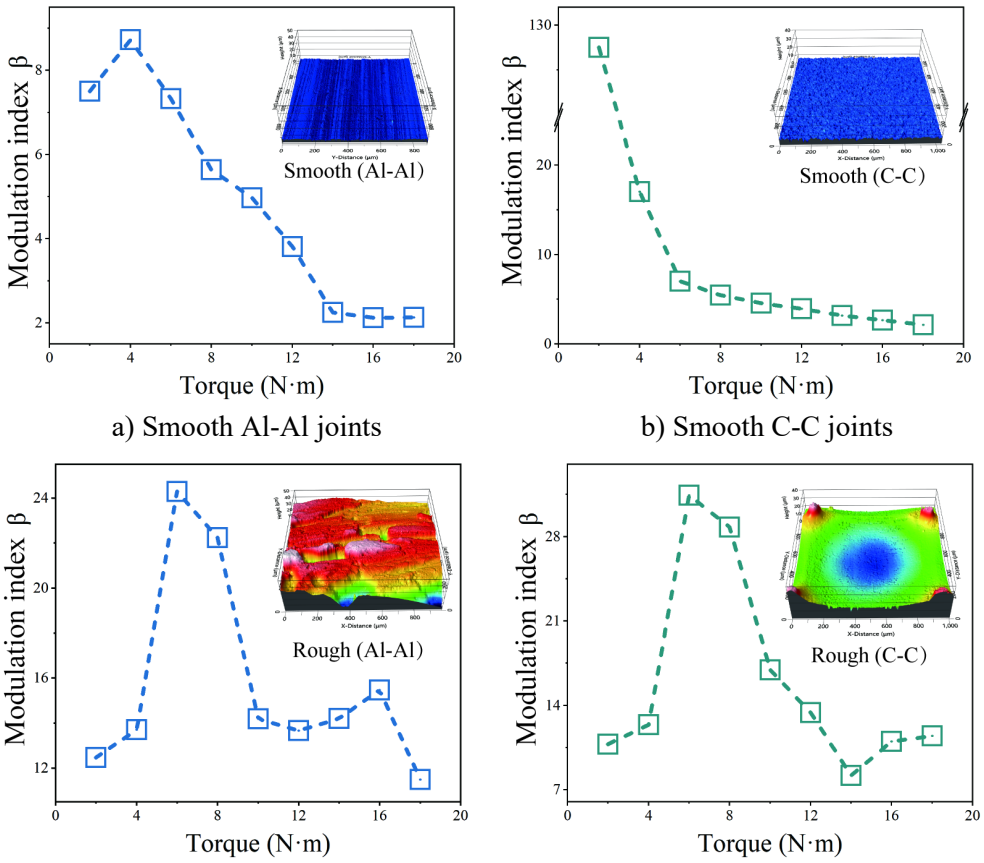

a) Smooth Al-Al joints b) Smooth C-C joints

c) Rough Al-Al joints d) Rough C-C joints

Fig. 9. Measured β over torques for joints with different surface.

The results for the two kinds of materials consistently indicate that the non-monotonic variations of β for the rough surface are more remarkable compared with that for the smooth surface. Furthermore, take CFRP for example, the material yielding strength for Figs. 9b and d are the same, but Fig. 9d shows the non-monotonic β in contrast to the monotonic β in Fig. 9b. Hence, the rough-surface contact nonlinearity is a significant factor leading to the non-monotonic VAM responses.

4.2 Influence of retightening

Since the rough-surface condition is a key factor affecting the monotonicity of nonlinear modulation index, the correlation between the rough-surface condition and the progress of bolt tightening is worth to investigate. Actually, the SHM of bolt loosening are always confronting the problems, such as repeated preloading and fretting wear, during their entire-life service. Hence, the change of the interfacial condition of a specimen in practice becomes rather complicated and repetitive.

20 retightening tests for CFRP plates with smooth and rough surfaces were conducted, respectively. For each material, two same specimens were used to conduct repeated tests. For each specimen, the joint was serially retightened by 20 times. In each cycle, the VAM signals were measured at the interval of the tightening step of the bolted joint, and then the bolt was fully loosed for the next-cycle retightening. The measurement setup was the same as that in

Section 3.1 (Fig. 6a). The interval for each retightening was larger than 10 minutes and the whole test for each specimen cost 3 days, so the residual plasticity due to unloading was not considered in this work. Another assumption is that the 20-times retightening for CFRP plates was not significant enough to cause any macrocracks or fatigue damages.

(1) Rough specimen

Figs. 10a and b show the measured nonlinear modulation index β during the retightening in the two repeated tests for the C-C joint with rough surfaces. There are three forms of the measured results in Figs. 10a and 11a, i.e., elastic stage (printed in green), elastic-plastic stage (printed in black) and their transitional stage (printed in yellow). In the elastic stage, β monotonically decreases with the increase of torque. In contrast, β in the elastic-plastic stage shows the remarkable non-monotonic patterns at the two sides of loading (i.e., low stress and high stress). As a transitional behavior, one-side non-monotonic pattern of β emerges at the curves between the other two sections. The typical figures of the three stages (1st, 10th and 20th cycle in Fig.10a) are shown in Figs. 10c~e. Every curve for β can be described and fitted by the proposed theoretical model to investigate the variation of model parameters (i.e., m_0 and n), as shown in Figs. 10f~g. Based on the obtained model parameters, the theoretical maximum range for monotonic VAM detection can be calculated by the proposed model (Eq. (15)), which is shown in Fig. 10h.

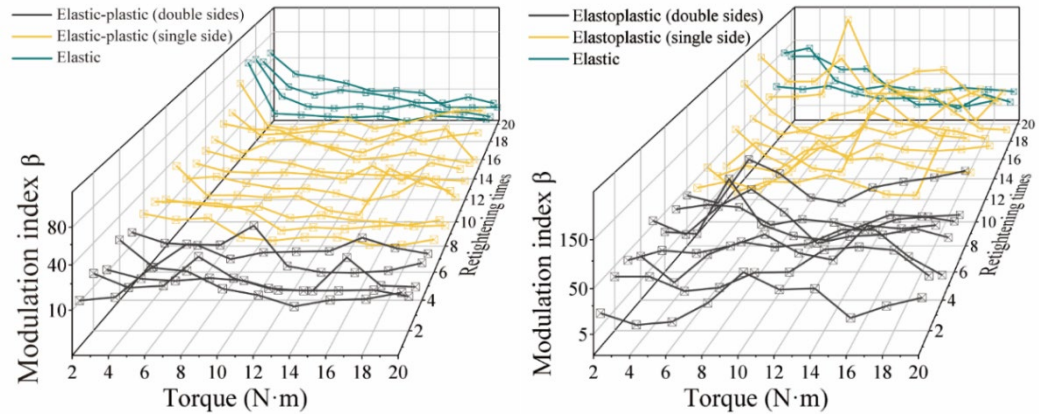

a) Measured β in the retightening (repeated test 1) b) Measured β in the retightening (repeated test 2)

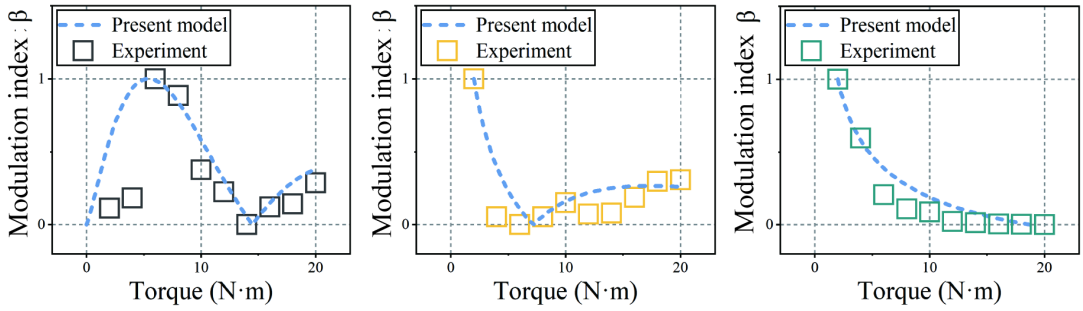

c) 1st cycle in Fig.10a (elastic-plastic) d) 10th cycle in Fig.10a (elastic-plastic) e) 20th cycle in Fig.10a (elastic)

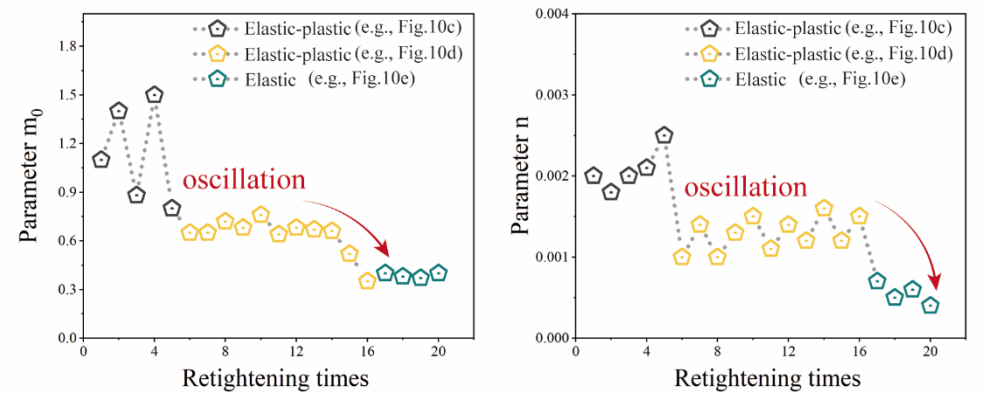

f) Variation of m_0 in Fig.10a g) Variation of n in Fig.10a

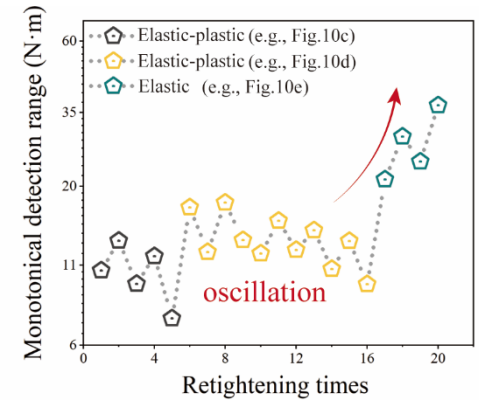

h) Theoretical maximum monotonical detection range for each cycle

Fig. 10. Results of retightening test for the rough specimen.

The two repeated tests for the rough surface (Figs. 10a and b) consistently show the gradual variation of β. At the beginning of the retightening, β shows a peak at the low-stress stage and a bounce at the high-stress stage, following the remarkable elastic-plastic behavior predicted by the proposed model. Then, with the increase of the retightening cycles, β indicates the transitional behavior of which the monotonic detection range keeps expanding. After the 17th retightening, β starts to show a monotonic decrease over the preload range from 0 to 20 N·m. The fitted model parameters in Figs. 10 f and g show the decreasing trend of n and m_0 for the rough specimen, which theoretically means, the roughness and plasticity of asperities have been gradually eliminated, resulting in the elastic behavior of β. The rough specimen initially has a shortest monotonic range lower than 12 N·m at the beginning of the retightening. However, after multiple retightening cycles, its theoretical ultimate monotonic range can reach up to 40 N·m (Fig. 10 h). Gong et al.[6] have also found that the polished surface shows a better result of VAM evaluation than the rough surface.

During the retightening test, the interfacial profile of the contact region with the area of 1 mm^2 was measured by the profile tester (Filmetrics®, Profilm 3D). Figs. 11 a~c show the interfacial profile of the specimen for Figs.10a before its 1st tightening, after its 15th tightening and after its 20th tightening respectively. Meanwhile, the regional statistical rough parameters (kurtosis Sku and arithmetic mean height Sa) for Figs. 11 a~c were obtained, where Sa represents the sectional mean height and Sku represents the sharpness of asperities.

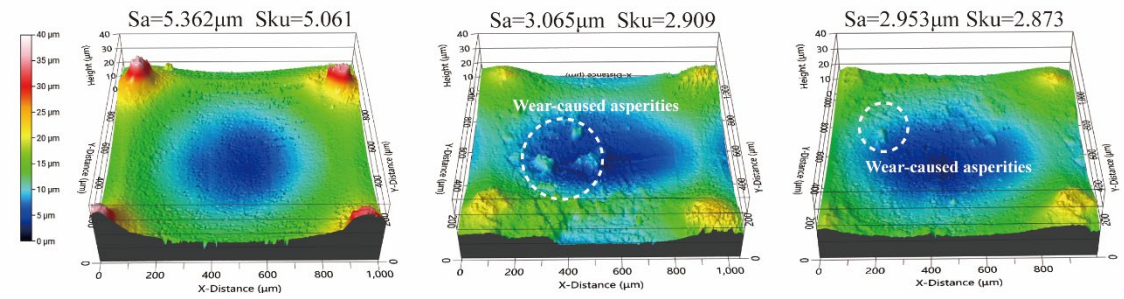

a) Before loading b) 15th cycle c) 20th cycle

Fig. 11. 3D profiles of the bolted region on the rough specimen during retightening test 1.

As shown in Fig.11, the outstanding rough asperities on the bolted region and the corresponding Sa and Sku gradually decrease with the increase of retightening cycles. That is because the accumulation of plastic deformation of the asperities under the repeated compression. The variation of the surface from rough state to smooth state and the loss of interfacial plasticity is consistent with the decrease of the model parameters (in Figs. 10 f and g), which has validated the theoretical frame. Meanwhile, in the repeated progress of tightness and looseness, it is inevitable that even the flat region will be worn to cause the small asperities. Such variation of interface is random and complicated in the cyclic loading [28], and is a significant factor of the oscillation of the model parameters and the monotonicity of β. In the case of rough specimen, the wear-caused asperities are much smaller than the manufactured asperities (at the corners of Fig.11), so their contribution to the VAM test is relatively slight.

(2) Smooth specimen

Figs. 12a and b show the measured nonlinear modulation index β during the retightening in the two repeated tests for the C-C joint with smooth surfaces. The experimental setup and the approach of factor analysis are the same as those for rough specimen.

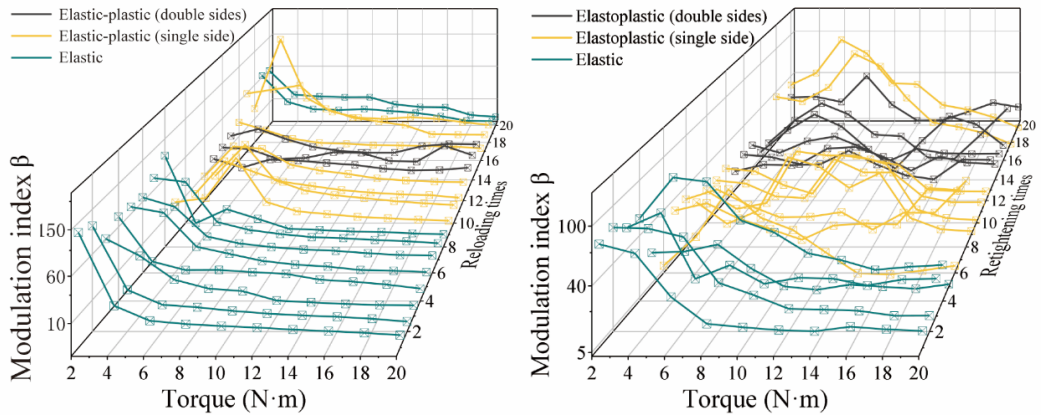

a) Measured β in the retightening (repeated test 1) b) Measured β I n the retightening (repeated test 2)

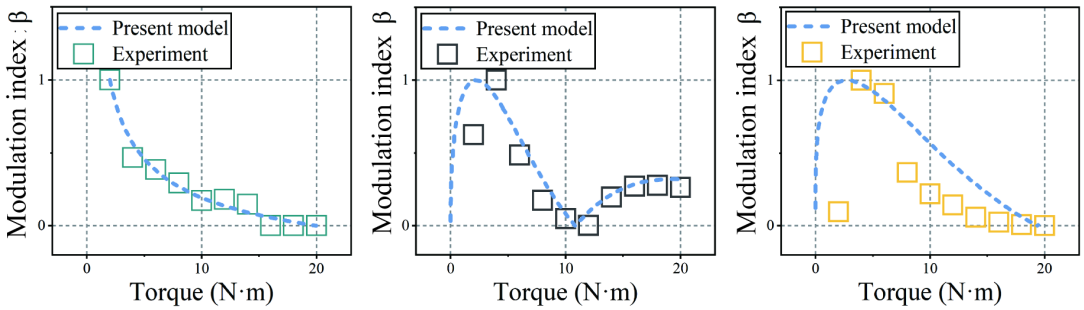

c) 1st cycle in Fig.12a (elastic) d) 15th cycle in Fig.12a (elastic-plastic) e) 10th cycle in Fig.12a (elastic-plastic)

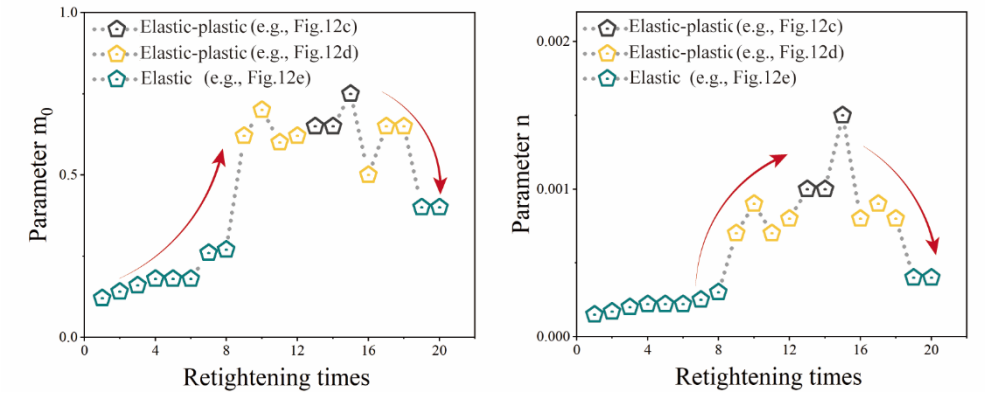

f) Variation of m_0 in Fig.12a g) Variation of n in Fig.12a

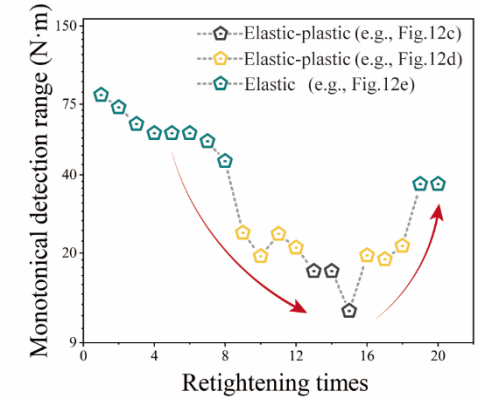

h) Theoretical maximum monotonical detection range for each cycle

Fig. 12. Results of retightening test for the smooth specimen.

For the smooth specimen, β in Fig. 12a and b monotonically decreases at the beginning of retightening. Then the following elastic-plastic curves before the 12th retightening still have wide decreasing ranges, in which only the single-side non-monotonic curves have emerged. The explanation for the results in Fig.12 can be obtained from the variation of interfacial profiles in Fig.13. The heights of the asperities at the unloaded surface are uniform, then, similar with Fig.11b, many peaks (higher than 10 μm) are caused due to wear during retightening (Fig. 12h). Unlike the wear-caused asperities on the rough surface, the asperities in Fig.13b are outstanding compared with the pristine regions. That is why the value of plate sharpness (represented by kurtosis Sku) for Fig.13b becomes higher than that for Figs. 13a and c, although the average height of asperities (Sa) keeps decreasing. Based on the present theoretical frame,

the rougher surface can lead to the more remarkable non-monotonicity of β, as is shown in Fig.12a and b. Zhao et al. [28] and Berthe et al. [29] have also reported the local rough asperity generated at the flat surface after loading, and explained as the accumulation of residual deformation.

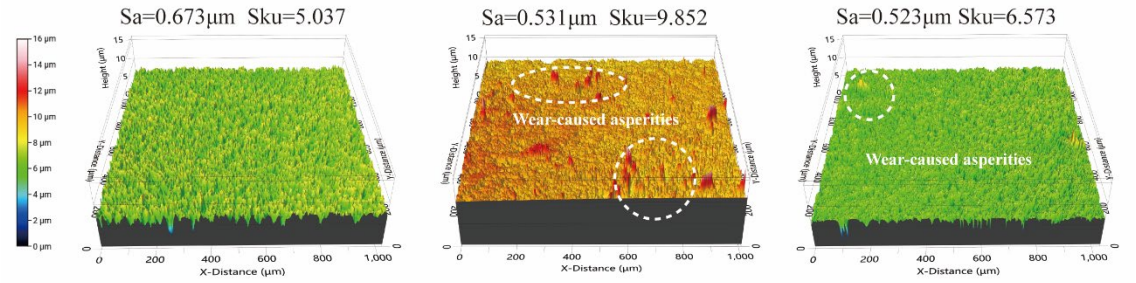

a) Before loading b) 15th cycle c) 20th cycle

Fig. 13. 3D profiles of the bolted region on the smooth specimen during retightening test 1.

We should note that after the emergence of double-sides elastic-plastic patterns (at about the 15th retightening), the repeated result in Fig.12b slightly differs from that in Fig.12a. In Fig.12a, the most significant elastic-plastic behavior (i.e., double-sides non-monotonic) has not shown for the rest of the retightening steps, and β has a wider monotonic range larger than 18 N·m (Fig. 12h). In contrast, although β at the 18th and 20th cycles in Fig. 12b shows single-side elastic-plastic behavior, the double-sides non-monotonic curve emerges again at the 19th cycle. Such a difference indicates the randomness of the roughness evolution of the interface [28]. As also reported by [29], the concurrent interfacial evolution is that the highest asperities on the rough surface will be shaved down, while the smooth and flat region will also be worn to generate new peaks.

However, the general tendency of β for Fig.12a and b is becoming more elastic and monotonic, and they are expected [30] to finally reach a steady and elastic state because the accumulation of the plastic deformation will cause the stiffness hardening of interfacial asperities. That is why the theoretical monotonic detection range for the smooth plate increases after reaching the lowest level (Fig. 12h). Therefore, for the practical application of VAM method, the rough-caused non-monotonicity is not persistent. Also, the decrease of monotonic detection range can be measured in the retightening test and predicted based on the proposed model, which helps adjust the arrangement of VAM-based SHM.

5 Conclusion

The full-range evaluation of bolt loosening based on VAM method was investigated. A new elastic-plastic model was proposed to explain the non-monotonic behaviors of the nonlinear features for the wide-range variation of the preload.

Based on the patterns of the elastic-plastic stiffness softening measured by the indentation test, a pressure-dependent exponent was used to modify the existing elastic power-law model. In the present model, the VAM responses at a joint depend on the combination of the initial rough

condition (represented by parameter m_0) and the softening property (represented by parameter n) of the contact asperities during tightening. The results predicted by the present model were validated through experiments and simulations, which indicated that the nonlinear modulation index shows an increase at the beginning of the preloading for a rougher interface (larger m_0), then followed by a power-law decrease as expected by the elastic model, and finally exhibits a bounce for the high-stress stage when the interfacial softening is significant (larger n).

The comparative experiment of plates made from CFRP and aluminum with different roughness indicated that the interfacial asperity characteristics of the bolted joint were the major factors leading to the non-monotonic VAM behaviors rather than the material yielding. The gradually varied trends for nonlinear modulation index in the torque monitoring were revealed through the retightening tests. The nonlinear modulation index for the smooth plate showed a better monotonicity than that for the rough plate at the beginning of retightening, but manifested a temporary non-monotonicity due to the fretting wear during the retightening process. Nevertheless, the nonlinear features for the two roughness conditions consistently showed monotonic behavior as their surfaces were finally smoothened down. During the retightening test, the rougher the interfacial condition becomes, the higher the parameters of present model rise to and the easier the nonlinear modulation index will turn to non-monotonic. In the lifetime service of the bolted joint, retightening of the loose bolt or interfacial fretting wear always happens. However, the monotonic detection range of the VAM method is expected to expand with the decrease of roughness, which manifests the unique potential of VAM method in the long-term SHM.

We should also note, in the aim of solving the application problem of VAM evaluation in bolt loosening, the present model simply describes the elastic-plastic VAM behavior by introducing a parameter to consider the thorough softening of interfacial asperities. Actually, the specific contributions of the roughness-caused plasticities (e.g., loading-unloading hysteresis, dislocation or hardening) is still worth to be further studied to improve the modelling accuracy. Additionally, the non-monotonicity of nonlinear features caused by material fatigue in the long-term SHM will be covered in the future work.

Acknowledgments

This research is sponsored by National Natural Science Foundation of China (NSFC) (12202313), Innovation Fund Project of the National Engineering and Research Center for Commercial Aircraft Manufacturing（COMACSFGS20221872）， Young Elite Scientists Sponsorship Program by CAST (2022QNRC001) and supported by the Fundamental Research Funds for the Central Universities from Tongji University.

CRediT authorship contribution statement

Jianbin Li: Methodology, Investigation, Writing - original draft. **Bo Wen**: Investigation. **Zhen Zhang**: Supervision. **Qian Li**: Resources. **Yi He**: Data curation. **Zhongqing Su**: Supervision.

Declaration of Competing Interest

The authors declare that they have no known competing financial interests or personal relationships that could have appeared to influence the work reported in this paper.

Reference

[1] X. Qin, C. Peng, G. Zhao, Z. Ju, S. Lv, M. Jiang, Q. Sui, L. Jia, Full life-cycle monitoring and earlier warning for bolt joint loosening using modified vibro-acoustic modulation, Mech. Syst. Sig. Process., 162 (2022). https://doi.org/10.1016/j.ymssp.2021.108054.

[2] F. Du, S. Wu, C. Xu, Z. Yang, Z. Su, Electromechanical Impedance Temperature Compensation and Bolt Loosening Monitoring Based on Modified Unet and Multitask Learning, IEEE Sens. J., 23 (2023) 4556-4567. https://doi.org/10.1109/jsen.2021.3132943.

[3] F. Du, S. Wu, S. Xing, C. Xu, Z. Su, Temperature compensation to guided wave-based monitoring of bolt loosening using an attention-based multi-task network, Struct. Health Monit., (2022). https://doi.org/10.1177/14759217221113443.

[4] J. Li, Y. He, Q. Li, Z. Zhang, Artificial Intelligence (AI)-Based Evaluation of Bolt Loosening Using Vibro-Acoustic Modulation (VAM) Features from a Combination of Simulation and Experiments, Applied Sciences, 12 (2022). https://doi.org/10.3390/app122412920.

[5] Z. Zhang, M. Liu, Z. Su, Y. Xiao, Quantitative evaluation of residual torque of a loose bolt based on wave energy dissipation and vibro-acoustic modulation: A comparative study, J. Sound Vib., 383 (2016) 156-170. https://doi.org/10.1016/j.jsv.2016.07.001.

[6] H. Gong, J. Huang, J. Liu, X. Deng, Proof-of-concept study of high-order sideband for bolt loosening detection using vibroacoustic modulation method, Mech. Syst. Sig. Process., 169 (2022). https://doi.org/10.1016/j.ymssp.2021.108638.

[7] F. Amerini, M. Meo, Structural health monitoring of bolted joints using linear and nonlinear acoustic/ultrasound methods, Struct. Health Monit., 10 (2010) 659-672.

[8] Z. Zhang, M. Liu, Y. Liao, Z. Su, Y. Xiao, Contact acoustic nonlinearity (CAN)-based continuous monitoring of bolt loosening: Hybrid use of high-order harmonics and spectral sidebands, Mech. Syst. Sig. Process., 103 (2018) 280-294. https://doi.org/10.1016/j.ymssp.2017.10.009.

[9] S. Biwa, S. Nakajima, N. Ohno, On the Acoustic Nonlinearity of Solid-Solid Contact With Pressure-Dependent Interface Stiffness, J. Appl. Mech., 71 (2004) 508-515. https://doi.org/10.1115/1.1767169.

[10] J.J. Meyer, D.E. Adams, Using impact modulation to quantify nonlinearities associated with bolt loosening with applications to satellite structures, Mech. Syst. Sig. Process., 116 (2019) 787-795. https://doi.org/10.1016/j.ymssp.2018.06.042.

[11] F. Wang, G. Song, Bolt early looseness monitoring using modified vibro-acoustic modulation by time-reversal, Mech. Syst. Sig. Process., 130 (2019) 349-360. https://doi.org/10.1016/j.ymssp.2019.04.036.

[12] F. Wang, G. Song, Monitoring of multi-bolt connection looseness using a novel vibro-acoustic method, Nonlinear Dyn., 100 (2020) 243-254. https://doi.org/10.1007/s11071-020-05508-7.

[13] N. Zhao, H. Linsheng, G. Song, Vibration acoustic modulation for bolt looseness

monitoring based on frequency-swept excitation and bispectrum, Smart Mater. Struct., 32 (2023). https://doi.org/10.1088/1361-665X/acb579.
[14] S.M.Y. Nikravesh, M. Goudarzi, Experimental and numerical looseness detection and assessment in flanged joints using vibro-acoustic modulation method, Mech. Based Des. Struct. Mach., 50 (2020) 1400-1416. https://doi.org/10.1080/15397734.2020.1753534.
[15] I.Y. Solodov, Ultrasonics of non-linear contacts: propagation, reflection and NDE-applications, Ultrasonics, 36 (1998) 383-390. https://doi.org/https://doi.org/10.1016/S0041-624X(97)00041-3.
[16] N. Li, J. Sun, J. Jiao, B. Wu, C. He, Quantitative evaluation of micro-cracks using nonlinear ultrasonic modulation method, NDT & E Int., 79 (2016) 63-72. https://doi.org/10.1016/j.ndteint.2015.12.003.
[17] K. Wang, M. Liu, Z. Su, S. Yuan, Z. Fan, Analytical insight into "breathing" crack-induced acoustic nonlinearity with an application to quantitative evaluation of contact cracks, Ultrasonics, 88 (2018) 157-167. https://doi.org/10.1016/j.ultras.2018.03.008.
[18] Y. He, Y. Xiao, Z. Su, Y. Pan, Z. Zhang, Contact acoustic nonlinearity effect on the vibro-acoustic modulation of delaminated composite structures, Mech. Syst. Sig. Process., 163 (2022). https://doi.org/10.1016/j.ymssp.2021.108161.
[19] D. Donskoy, D. Liu, Vibro-acoustic modulation baseline-free non-destructive testing, J. Sound Vib., 492 (2021). https://doi.org/10.1016/j.jsv.2020.115808.
[20] G. Raghunath, B. Barkley, A.B. Flatau, Smart washers to measure bolt loads using Magnetostrictive Galfenol, 23rd AIAA Adaptive Structures Conference, 5-9 Jan. 2015, American Institute of Aeronautics and Astronautics Inc., Reston, VA, USA, 2015, pp. 6 pp.
[21] D. Broda, W.J. Staszewski, A. Martowicz, T. Uhl, V.V. Silberschmidt, Modelling of nonlinear crack–wave interactions for damage detection based on ultrasound—A review, J. Sound Vib., 333 (2014) 1097-1118. https://doi.org/10.1016/j.jsv.2013.09.033.
[22] J.-Y. Kim, J.-S. Lee, A micromechanical model for nonlinear acoustic properties of interfaces between solids, J. Appl. Phys., 101 (2007) 043501. https://doi.org/10.1063/1.2434939.
[23] Drinkwater, B., W., Dwyer-Joyce, R., S., Cawley, P., A Study of the Interaction between Ultrasound and a Partially Contacting Solid--Solid Interface, Proceedings of the Royal Society A: Mathematical, (1996).
[24] C. Pecorari, M. Poznic, On the linear and nonlinear acoustic properties of dry and water-confining elasto-plastic interfaces, Proceedings of the Royal Society A: Mathematical, Physical and Engineering Sciences, 462 (2005) 769-788. https://doi.org/10.1098/rspa.2005.1595.
[25] C. Pecorari, Adhesion and nonlinear scattering by rough surfaces in contact: Beyond the phenomenology of the Preisach–Mayergoyz framework, The Journal of the Acoustical Society of America, 116 (2004) 1938-1947. https://doi.org/10.1121/1.1785616.
[26] Z. Zhang, H. Xu, Y. Liao, Z. Su, Y. Xiao, Vibro-acoustic modulation (VAM)-inspired structural integrity monitoring and its applications to bolted composite joints, Compos. Struct., 176 (2017) 505-515. https://doi.org/10.1016/j.compstruct.2017.05.043.
[27] D. Liu, D. Donskoy, Cross-correlation vibro-acoustic modulation method for damage detection, Struct. Health Monit., (2023). https://doi.org/10.1177/14759217231177005.
[28] H. Zhao, W. Ta, and Y. Zhou, The mechanical-thermal-electrical contact behaviors between rough surfaces under cyclic loading, Acta Mech. Sin. 39,123212 (2023),

https://doi.org/10.1007/s10409-023-23212-x.
[29] L. Berthe, P. Sainsot, A.A. Lubrecht, M.C. Baietto, Plastic deformation of rough rolling contact: An experimental and numerical investigation, Wear, 312 (2014) 51-57. https://doi.org/10.1016/j.wear.2014.01.017.
[30] A. Kapoor, K.L. Johnson, Effect of changes in contact geometry on shakedown of surfaces in rolling/sliding contact, International Journal of Mechanical Sciences, 34 (1992) 223-239. https://doi.org/10.1016/0020-7403(92)90073-P.